Inorganic Chemistry

Article

pubs.acs.org/IC

Chloride Ion-Aided Self-Assembly of Pseudoclathrochelate Metal Tris-pyrazoloximates

Oleg A. Varzatskii,[†] Larysa V. Penkova,[‡] Svitlana V. Kats,[‡] Alexander V. Dolganov,[§] Anna V. Vologzhanina,[§] Alexander A. Pavlov,[§] Valentin V. Novikov,[§] Artem S. Bogomyakov,[⊥] Victor N. Nemykin,[∥] and Yan Z. Voloshin*[,§]

[†]Vernadskii Institute of General and Inorganic Chemistry of the National Academy of Sciences of Ukraine, 03680 Kyiv, Ukraine

[‡]Kyiv National Taras Shevchenko University, 01601 Kyiv, Ukraine

[§]Nesmeyanov Institute of Organoelement Compounds of the Russian Academy of Sciences, 119991 Moscow, Russia

[⊥]International Tomography Center, Siberian Branch of the Russian Academy of Sciences, 630090 Novosibirsk, Russia

[∥]Department of Chemistry & Biochemistry, University of Minnesota Duluth, Duluth, Minnesota 55812, United States

Supporting Information

ABSTRACT: Chloride ion-aided one-pot template self-assembly of a mixed pyrazoloxime ligand with phenylboronic acid on a corresponding metal(II) ion as a matrix afforded the first boron-capped zinc, cobalt, iron, and manganese pseudoclathrochelate tris-pyrazoloximates. The presence of a pseudocross-linking hydrogen-bonded chloride ion is critical for their formation, as the same chloride-capped complexes were isolated even in the presence of large excesses of bromide and iodide ions. As revealed by X-ray diffraction, all complexes are capped with a chloride ion via three N−H···Cl hydrogen bonds that stabilize their pseudomacrobicyclic frameworks. The MN_6 coordination polyhedra possess a distorted trigonal prismatic geometry, with the distortion angles φ between their nonequivalent N_3 bases of approximately 0°. Temperature dependences of the effective magnetic moment for the paramagnetic complexes showed the encapsulated metal(II) ions to be in a high-spin state in the temperature range of 2−300 K. In the case of the iron(II) pseudoclathrochelate, density functional theory (DFT) and time-dependent DFT calculations were used to assess its spin state as well as the ^{57}Fe Mössbauer and UV−vis−NIR parameters. Cyclic voltammetry studies performed for these pseudomacrobicyclic complexes showed them to undergo irreversible or quasi-reversible metal-localized oxidations and reductions. As no changes are observed in the presence of a substantial excess of bromide ion, no anion-exchange reaction occurs, and thus the pseudoclathrochelates have a high affinity toward chloride anions in solution.

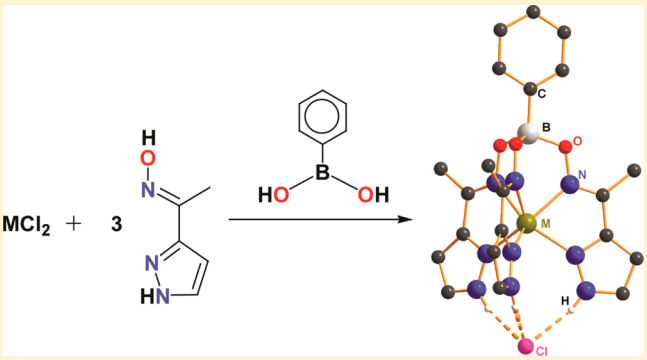

1. INTRODUCTION

Most of the known cage metal complexes with polyazomethine quasi-aromatic macrobicyclic frameworks (clathrochelates,[1] Scheme 1, **1** and **2**) have been synthesized via one-pot self-assembly of corresponding chelating ligands and capping (cross-linking) agents on a metal ion as a matrix. In case of symmetric ligands with equivalent donor groups, this allowed obtaining clathrochelate complexes mainly with the same apical tripodal moieties and chelate ribbed fragments. At the same time, the use of ligands with substantially nonequivalent donor fragments (and, therefore, with different reactivity) made it possible to synthesize a variety of polytopic and hybrid molecular and supramolecular systems by their stepwise assembling. A wide range of clathrochelates has been thus obtained, starting from oximehydrazonate ligands with non-equivalent oxime and hydrazone donor groups[2] using their different reactivity for the above stepwise synthesis. In particular, template condensation of oximehydrazones with corresponding Lewis acids (i.e., boron-,[2a−c,g,j−m] tin-,[2e] germanium-,[2f,h] and antimony-containing[2d] cross-linking agents) afforded semiclathrochelate complexes; condensation with active carbonyl-containing agents via their reactive hydrazonate donor groups gave the target clathrochelates with 1,3,5-triazacyclohexane capping fragment (Scheme 1, **2**).

Recently, hybrid dioximatopyrazoloximate macrocyclic and macrobicyclic (clathrochelatoscorpionate) complexes (Scheme 1, **3** and **4**, respectively), the derivatives of a mixed pyrazoloxime ligand PzOxH, were synthesized;[3] however, their properties are mainly governed by two α-benzyldioximate chelate fragments. Here we describe the first boron-capped metal tris-pyrazoloximates with an unusual pseudomacrobicyclic encapsulating ligand (Scheme 1, **5**).

Received: November 22, 2013
Published: February 21, 2014

   dx.doi.org/10.1021/ic4029047 | *Inorg. Chem.* 2014, 53, 3062−3071

Scheme 1. Some Cage Complexes and Their Macrocyclic and Pseudomacrobicyclic Analogs

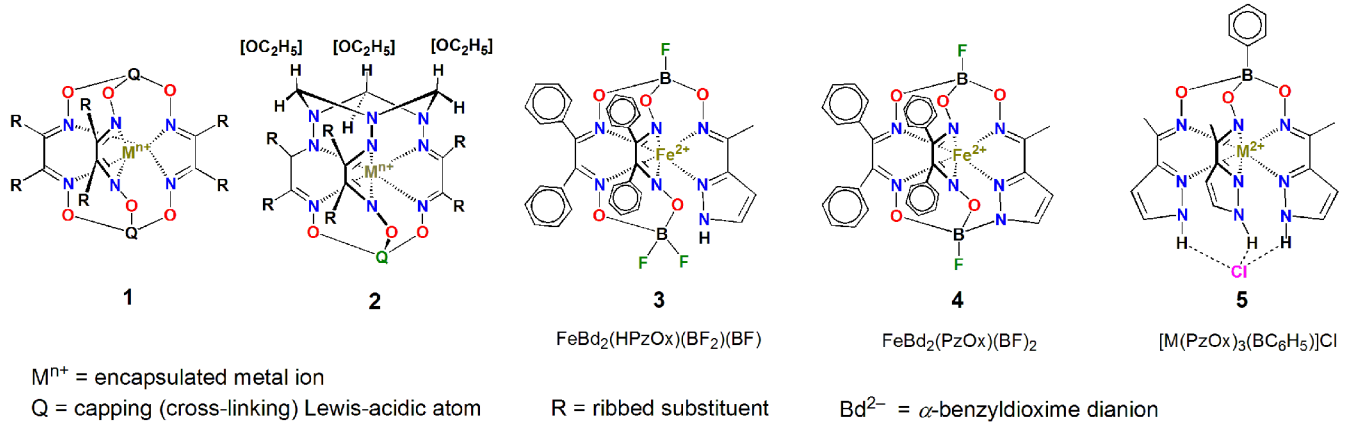

2. EXPERIMENTAL SECTION

Materials and Physical Measurements. The reagents used, $FeCl_2{\cdot}4H_2O$, $CoCl_2{\cdot}6H_2O$, $MnCl_2{\cdot}4H_2O$, anhydrous $ZnCl_2$, phenylboronic acid, sorbents, organic bases, and solvents, were obtained commercially (SAF). The pyrazoloxime ligand PzOxH was prepared as described in reference 3.

Analytical data (C, H, N contents) were obtained with a Carlo Erba model 1106 microanalyzer.

MALDI-TOF mass spectra were recorded using a MALDI-TOF-MS Bruker Autoflex II (Bruker Daltonics) mass spectrometer in reflectomol mode. The ionization was induced by UV-laser with wavelength 337 nm. The samples were applied to a nickel plate, and 2,5-dihydroxybenzoic acid was used as the matrix. The accuracy of measurements was 0.1%.

Infrared (IR) spectra of the solid samples (KBr tablets) in the range of 400−4000 cm^{-1} were recorded with a Perkin-Elmer FT-IR Spectrum BX II spectrometer.

Ultraviolet−visible (UV−vis) spectra of solutions in dichloromethane were recorded in the range of 230−900 nm with a Lambda 9 Perkin-Elmer spectrophotometer. The individual Gaussian components of these spectra were calculated using the SPECTRA program. Visible−near-IR (vis−NIR) spectra of solutions in chloroform were recorded in the range of 700−2500 nm with Tensor 37 Bruker FT- and Jasco V-670 spectrophotometers.

^1H and ^{13}C NMR spectra were recorded from CD_2Cl_2 and $CDCl_3$ solutions with a Bruker Avance 600 spectrometer. The measurements were done using the residual signals of deuterated solvents (CD_2Cl_2: ^1H 5.32 ppm, ^{13}C 53.8 ppm; $CDCl_3$: ^1H 7.25 ppm, ^{13}C 77.0 ppm).

^{57}Fe Mössbauer absorption spectra of the iron complex were recorded at 77 and 298 K using a NP-255 spectrometer (Hungary) with a constant acceleration mode and a symmetrical triangular change in the velocity of a γ-quantum source (^{57}Co in a rhodium matrix with an activity equal to 5 mCu and with a line emission width equal to 0.11 mm s^{-1}). The spectra were collected with a 511-multichannel analyzer. The speed scale of the spectrometer was calibrated using the spectrum of sodium nitroprusside as a standard. The isomeric shift (IS) value was obtained relative to the center of this spectrum.

Cyclic voltammetry (CV) experiments were carried out in dichloromethane solutions with 0.1 M $((n\text{-}C_4H_9)_4N)(BF_4)$ as supporting electrolyte, using a model Parstat 2273 (Prinston Applied Research, USA) potentiostat with a conventional and one-compartment three-electrode cell (10 mL of solution). A platinum disk electrode with an active surface area of 0.125 cm^2 was used as a working electrode. The electrode was thoroughly polished and rinsed before measurements. A platinum counter electrode and standard $Ag/AgCl/KCl_{aq}$ reference electrode (RE) were applied. All solutions were thoroughly de-aerated by passing argon through the solution before the CV experiments and above the solution during the measurements.

The magnetic susceptibility of the polycrystalline samples was measured with a Quantum Design MPMS*XL* SQUID magnetometer in the temperature range of 2−300 K, with magnetic field of up to 5 kOe. None of complexes exhibited any field dependence of molar magnetization at low temperatures. The diamagnetic corrections were made using the Pascal constants. The effective magnetic moment was calculated as $\mu_{eff}(T) = [(3k/N_A\mu_B^2)\chi T]^{1/2} \approx (8\chi T)^{1/2}$.

Single-Crystal X-ray Analysis. Single crystals of the complexes $[Fe(PzOx)_3(BC_6H_5)]Cl{\cdot}C_2H_5OH$ and $[Mn(PzOx)_3(BC_6H_5)]Cl{\cdot}C_2H_5OH$ were grown at room temperature (r.t.) from a dichloromethane−hexane−ethanol mixture; those of the pseudoclathrochelate $[Co(PzOx)_3(BC_6H_5)]Cl{\cdot}CHCl_3$ and $[Zn(PzOx)_3(BC_6H_5)]Cl{\cdot}CHCl_3$ were grown from a chloroform−hexane mixture. The intensities of reflections were measured at 100(2) K with a Bruker Apex II CCD diffractometer using graphite monochromated Mo Kα radiation (λ = 0.71073 Å). Transmission coefficients were determined using the SADABS program.[4] The structures were solved by the direct method and refined by full-matrix least-squares against F^2. Non-hydrogen atoms were refined in anisotropic approximation. The unit cell of the crystal $[Fe(PzOx)_3(BC_6H_5)]Cl{\cdot}C_2H_5OH$ contains highly disordered solvate ethanol molecules, which were treated as a diffuse contribution to the overall scattering without specific atom positions by SQUEEZE/PLATON;[5] the chemical formula, formula weight, and density were calculated, taking the solvate molecules into account. The solvate ethanol molecules in the crystal $[Mn(PzOx)_3(BC_6H_5)]Cl{\cdot}C_2H_5OH$ were refined with fixed C−O and C−C distances. Positions of the H(C) atoms were calculated geometrically, and those of H(N) atoms were located on Fourier maps. Hydrogen atoms were included in the refinement by the riding model with $U_{iso}(H) = nU_{eq}(C)$, where n = 1.5 for methyl groups and 1.2 for the other atoms. All calculations were made using the SHELXTL PLUS 5 program package.[6] The crystallographic data and experimental details are listed in Table S1 (see Supporting Information).

Computational Details. All computations were performed using Gaussian 09 software package running under Windows or UNIX OS.[7] Molecular orbital (MO) contributions were compiled from single-point calculations, using the QMForge program.[8] In all geometry optimizations and single-point calculations, the hybrid B3LYP exchange-correlation functional[9] was used. To account for the electrostatic contribution of chloride counterion to the density functional theory (DFT)-predicted ^{57}Fe Mössbauer spectral parameters, all computational work was conducted on the neutral ion pair. In geometry optimizations, X-ray diffraction data for the complex $[Fe(PzOx)_3(BC_6H_5)]Cl$ were used as a starting point with standard 6-311++G(2d) basis set for chloride anion[10] to ensure an accurate description of cation−anion interactions. Wachter's full-electron basis set[11] was used for the iron atom, while the 6-311G(d) basis set[12] was employed for all other atoms during geometry optimization. All three possible spin states (s = 2, s = 1, and s = 0) of this pseudoclathrochelate were considered during the geometry optimization. Default convergence criteria for the geometry optimization were used as implemented into the Gaussian 09 program.[7] Although all three geometry optimizations were carried out without any symmetry

dx.doi.org/10.1021/ic4029047 | Inorg. Chem. 2014, 53, 3062−3071

restraints, in all cases the geometries converged to C_s point group. In the case of the high-spin state ($s = 2$), DFT-optimized geometry was in a good agreement with the experimental X-ray diffraction data (see Supporting Information, Table S3). The vibronic frequencies were calculated for all optimized geometries to ensure convergence to a local minimum on the potential energy surface. In the case of single-point calculations, the Wachter's full-electron basis set[11] was decontracted as previously described[12,13] to facilitate an accurate electron density description at the iron center. DFT-predicted ISs for the optimized geometries with $s = 2$, $s = 1$, and $s = 0$, as well as that of the X-rayed complex with $s = 2$, were obtained from the electron-density values at the iron nucleus and calculated using the calibration equations as described previously by Hadt and Nemykin.[13] Quadrupole splitting value QS and symmetry parameter η were calculated directly from the electric field gradient (EFG) values of tensor components using the following equations: $QS = 1/2\ e\ Q\ V_{zz}\ (1 + \eta^2/3)^{1/2}$ and $\eta = (V_{xx} - V_{yy})/V_{zz}$, using constants described earlier.[13] A combination of the Wachter's full-electron basis set for iron atom(s) and the 6-311G(d) basis set[11,12] for all other atoms was used for the time-dependent (TD) DFT calculations. TDDFT calculations were conducted for the geometrically optimized structure of the complex $[Fe(PzOx)_3(BC_6H_5)]Cl$ ($s = 2$) for the first 50 excited states to ensure that all charge-transfer (CT) transitions of interest were calculated. Only positive excitation energies were found in the TDDFT calculations, suggesting that the self-consistent field (SCF) solution represented the ground state.

Syntheses. *$[Co(PzOx)_3(BC_6H_5)]Cl$.* Pyrazoloxime PzOxH (2.5 g, 20 mmol) and phenylboronic acid (1.17 g, 7.3 mmol) were dissolved in dry ethanol (20 mL) with intensive stirring under argon, and $CoCl_2 \cdot 6H_2O$ (1.58 g, 6.7 mmol) and $NaHCO_3$ (0.57 g, 6.7 mmol) were added. The reaction mixture was refluxed for 30 min and cooled to r.t., and the dark-orange precipitate formed was filtered off. The precipitate was washed with ethanol, diethyl ether, and hexane and dried in vacuo. The orange pseudoclathrochelate product was extracted from this solid with dichloromethane; the dichloromethane solution obtained was filtered off and rotary evaporated to dryness. Yield: 3.9 g (75%). Anal. Calcd for $C_{21}H_{23}N_9O_3BClCo$ (%): C, 45.47; H, 4.18; N, 22.73. Found (%): C, 45.32; H, 4.07; N, 22.54. ^{1}H NMR (CD_2Cl_2) δ 268.75 (br. s, 3H, NH), 85.08 (br. s, 3H, 5-Pz), 75.56 (br. s, 2H, *ortho*-Ph), 33.06 (br. s, 2H, *meta*-Ph), 28.26 (br. s, 1H, *para*-Ph), −7.46 (br. s, 3H, 4-Pz), −14.25 (br. s, 9H, CH_3). ^{13}C NMR (CD_2Cl_2) δ 827.4 (br. s, 5-Pz), 291.3 (s, CH_3), 288.7 (br.s, 4-Pz), 218.9 (s, *ortho*-Ph), 210.2 (s, *ipso*-Pz), 188.7 (br. s, *ipso*-Ph), 169.6 (s, *meta*-Ph), 159.1 (s, *para*-Ph), −436.2 (s, CH_3−C═N). MS (MALDI-TOF) m/z (I, %): 395 (100) $[M-PzOx-Cl^-]^+$, 519(40) $[M-Cl^-]^+$. IR (KBr) ν/cm^{-1}: 915, 936, 977, 1069, 1090, 1115, 1165 ν(N−O), 1217−1238m ν(B−O), 1530 {ν(C═N) + ν(C═C), Pz}, 1563, 1571 {ν(C═N), Ox}, 1645m {ν(C═N) + ν(C═C), Pz}. UV−vis (CH_2Cl_2): λ_{max}/nm ($\varepsilon \times 10^{-3}$ mol^{-1} L cm^{-1}) 247 (17), 261 (11), 283 (6.7), 317 (2.6), 346 (0.4), 434 (0.2), 486 (0.01). NIR ($CHCl_3$) λ_{max}/nm (ε, mol^{-1} L cm^{-1}) 1081 (7.1).

$[Fe(PzOx)_3(BC_6H_5)]Cl$. This complex was obtained like the previous one except that $FeCl_2 \cdot 4H_2O$ (1.33 g, 6,7 mmol) was used instead of $CoCl_2 \cdot 6H_2O$. Yield of the light-yellow fine-crystalline product was 2.12 g (64%). Anal. Calcd for $C_{21}H_{23}N_9O_3BClFe$ (%): C, 45.73; H, 4.20; N, 22.85. Found (%): C, 45.65; H, 4.07; N, 22.74. ^{1}H NMR ($CDCl_3$) δ 49.91 (br. s, 9H, CH_3), 42.71 (br. s, 3H, HC═CH), 27.33 (br. s, 3H, NH), 23.73 (br. s, 3H, HC═CH), 6.88, 6.41 (all br. s, 5H, Ph). ^{13}C NMR (CD_2Cl_2) δ 784.80 (s, 5-Pz), 326.15 (s, *ipso*-Pz), 286.38 (s, 4-Pz), 152.83 (s, CH_3), 145.17 (s, *ortho*-Ph), 130.42(s, *meta*-Ph), 125.38 (s, *para*-Ph), 69.36 (br. s, *ipso*-Ph), −310.32 (s, CH_3−C═N). MS (MALDI-TOF) m/z (I, %): 392(100) $[M-PzOx-Cl^-]^+$, 516(75) $[M-Cl^-]^+$. IR (KBr) ν/cm^{-1}: 939, 974, 1068, 1086, 1115, 1163 ν(N−O), 1215m ν(B−O), 1533 {ν(C═N) + ν(C═C), Pz}, 1568 {ν(C═N), Ox}, 1649 {ν(C═N) + ν(C═C), Pz}. UV−vis (CH_2Cl_2): λ_{max}/nm ($\varepsilon \times 10^{-3}$ mol^{-1} L cm^{-1}) 247 (19), 260 (5.2), 264 (1.5), 296 (5.4), 326 (0.7), 369 (0.4). NIR ($CHCl_3$) λ_{max}/nm ($\varepsilon \times 10^{-3}$ mol^{-1} L cm^{-1}) 905 (0.005). ^{57}Fe Mössbauer spectra (mm s^{-1}): IS = 1.232, QS = 3.447 (298 K); IS = 1.351, QS = 4.141 (77 K).

$[Zn(PzOx)_3(BC_6H_5)]Cl$. This complex was obtained like the pseudomacrobicycle $[Co(PzOx)_3(BC_6H_5)]Cl$, except that anhydrous $ZnCl_2$ (0.92g, 6.7 mmol) was used instead of $CoCl_2 \cdot 6H_2O$. Yield of the white fine-crystalline product was 2.63g (75%). Anal. Calcd for $C_{21}H_{23}N_9O_3BClZn$ (%): C, 44.95; H, 4.13; N, 22.47. Found (%): C, 44.85; H, 3.95; N, 22.34. ^{1}H NMR ($CDCl_3$) δ 14.71 (s, 3H, NH), 7.79 (m, 2H, *ortho*-Ph), 7.79 (s, 3H, 5-Pz), 7.33 (m, 2H, *meta*-Ph), 7.33 (m, 1H, *para*-Ph), 6.51 (s, 3H, 4-Pz), 2.31 (s, 9H, CH_3). ^{13}C NMR ($CDCl_3$) δ 147.79 (s, CH_3−C═N), 147.15 (s, *ipso*-Pz), 140.00 (br. s, *ipso*-Ph), 132.30 (s, *ortho*-Ph), 132.20 (s, 5-Pz), 127.43 (s, *meta*-Ph), 127.24 (s, *para*-Ph), 103.56 (s, 4-Pz), 11.72 (s, CH_3). MS (MALDI-TOF) m/z (I, %): 437 $[M-PzOx]^+$, 525(5) $[M-Cl^-]^+$. IR (KBr) ν/cm^{-1}: 945, 977, 1071, 1092, 1113, 1165 ν(N−O), 1215−1235m ν(B−O), 1541 {ν(C═N) + ν(C═C), Pz}, 1560, 1577 {ν(C═N), Ox}, 1653 {ν(C═N) + ν(C═C), Pz}. UV−vis (CH_2Cl_2): λ_{max}/nm ($\varepsilon \times 10^{-3}$ mol^{-1} L cm^{-1}) 246 (16), 254 (14), 268 (7.2), 289 (7.0), 303 (1.6).

$[Mn(PzOx)_3(BC_6H_5)]Cl$. This complex was obtained like the pseudomacrobicycle $[Co(PzOx)_3(BC_6H_5)]Cl$ one, except that $MnCl_2 \cdot 4H_2O$ (1.33g, 6.7 mmol) was used instead of $CoCl_2 \cdot 6H_2O$. Yield of the yellowish fine-crystalline product was 2.83g (82%). Anal. Calcd for $C_{21}H_{23}N_9O_3BClMn$ (%): C, 45.75; H, 4.18; N, 22.87. Found (%): C, 45.64; H, 4.34; N, 22.69. ^{1}H NMR ($CDCl_3$) δ 67.32 (br. s, 3H, NH), 40.29 (br. s, 3H, Pz), 27.50 (br. s, 3H, Pz), 7.36 (br. s, 5H, Ph), 2.15 (br. S, 9H, CH_3). ^{13}C NMR ($CDCl_3$) δ 207.09 (s, Pz), 144.89 (s, Pz), 130.93, 128.04, 127.32 (all s, Ph), 31.01 (s, CH_3). MS (MALDI-TOF) m/z: 515 $[M-Cl^-]^+$. IR (KBr) ν/cm^{-1}: 935, 947, 974, 1069, 1085, 1113, 1161 ν(N−O), 1212−1229m ν(B−O), 1526 {ν(C═N) + ν(C═C), Pz}, 1562, 1580 {ν(C═N), Ox}, 1654 {ν(C═N) + ν(C═C), Pz}. UV−vis (CH_2Cl_2): λ_{max}/nm ($\varepsilon \times 10^{-3}$ mol^{-1} L cm^{-1}) 246 (12), 261 (18), 280 (9.9), 296 (5.4), 307 (3.3), 371 (0.028), 419 (0.025), 476 (0.009).

3. RESULTS AND DISCUSSION

Synthesis. Easy and efficient self-assembly of zinc, cobalt, iron, and manganese(II) pseudoclathrochelates was performed in mild conditions by one-pot template condensation of the mixed pyrazoloxime ligand PzOxH having significantly non-equivalent donor groups with phenylboronic acid as a capping Lewis-acidic agent on the corresponding metal ion as a matrix (Scheme 2); such general synthetic approach is characteristic of

Scheme 2. Synthesis of the Pseudoclathrochelate Metal Tris-Pyrazoloximates

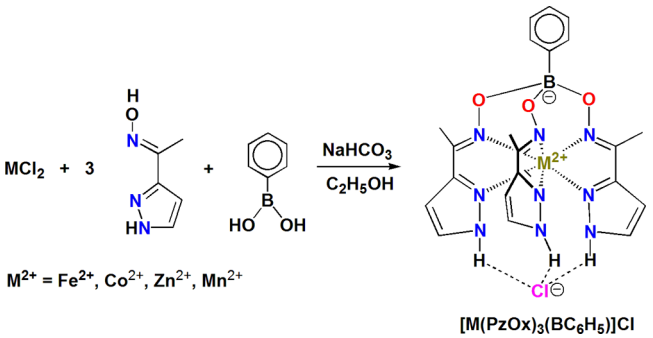

the clathrochelate chemistry.[1] In this case, however, hydrogen atoms of three terminal pyrazolyl NH groups form a pseudomacrobicyclic ligand via their hydrogen bonding with a chloride counterion $Cl^-\cdots(HN)_3$, thus encapsulating the corresponding metal ion (vide infra). As a result, three additional six-membered pseudochelate cycles are formed in a tripodal tris-pyrazolyl fragment.

Hydrogen bonding of halogen ions with nitrogen-containing heterocyclic groups has been widely used for halogen ion

dx.doi.org/10.1021/ic4029047 | Inorg. Chem. 2014, 53, 3062−3071

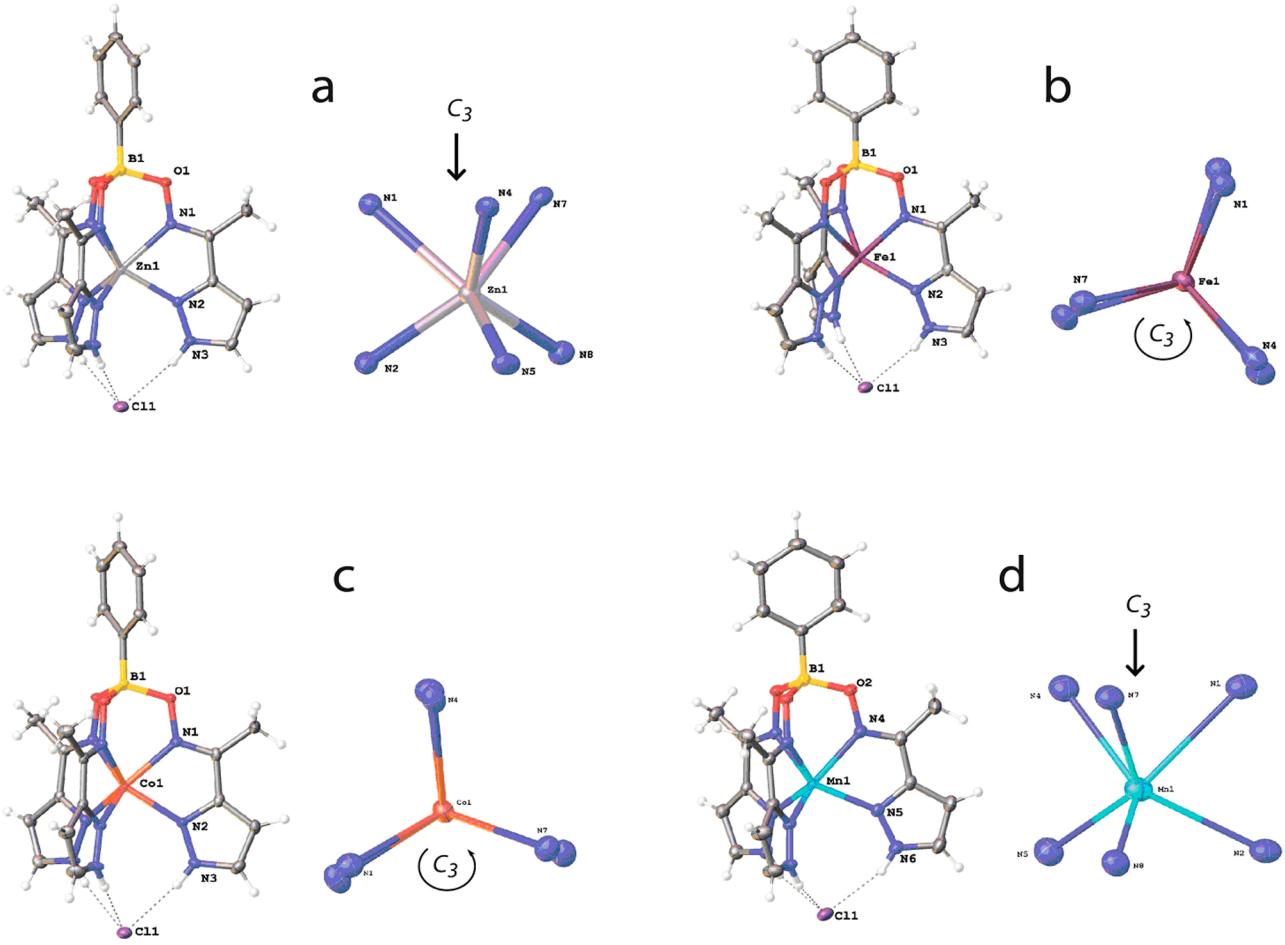

Figure 1. General views of the pseudomacrobicyclic ionic associates $[M(PzOx)_3(BC_6H_5)]Cl$ {where M^{2+} is (a) Zn^{2+}, (b) Fe^{2+}, (c) Co^{2+}, and (d) Mn^{2+}} and those of their MN_6-coordination polyhedra {(a,d) the side views and (b,c) the projections along their C_3-pseudoaxis} given in thermal ellipsoids drawn at p = 50%.

binding, recognition, and detection.[14] Indeed, we failed to obtain the pseudomacrobicyclic complexes in the absence of chloride ions in the reaction mixture, for example, either starting from tetrafluoroborate salts of these metal ions or using nonhalogen-containing ionic liquids as a solvent instead of ethanol. Thus, the presence of the capping (cross-linking) chloride ion is critical for their formation; the same chloride-capped complexes were isolated even in the presence of 10 M excesses of bromide and iodide ions. Note that, by using the 3d metal(II) bromides instead of their chlorides, we failed to obtain the corresponding pseudomacrobicyclic complexes in various reaction conditions.

Spectral Studies. The complexes obtained were thoroughly characterized using elemental analysis, MALDI-TOF mass spectrometry, IR, UV−vis, ^{57}Fe Mössbauer (for an iron complex), ^{1}H and ^{13}C NMR spectroscopy, and SQUID magnetometry.

The spin state of paramagnetic ions in these pseudoclathrochelates was determined by SQUID magnetometry (see Supporting Information, Figure S1). All the complexes were high-spin in the temperature range of 5−300 K, with s = 3/2, 2, and 5/2 in the case of cobalt, iron, and manganese(II) compounds, respectively (see Supporting Information for more details).[15] The high-spin state of the encapsulated iron(II) ion in its complex $[Fe(PzOx)_3(BC_6H_5)]Cl$ also follows from the ^{57}Fe Mössbauer parameters (see Experimental Section).

Magnetic properties of these compounds can be additionally characterized by NMR spectroscopy, allowing detailed insight into their structure.[16] As NMR signals of paramagnetic compounds are usually significantly shifted and broadened, the assignment of signals was not trivial, so it was assisted by DFT calculations (see Supporting Information), which will be published elsewhere. The NMR paramagnetic shifts depend on both the geometry and electronic structure of a compound,[17] with a dipolar mechanism of interaction leading to pseudocontact shifts, which directly depend on purely geometrical parameters, while direct contact interaction gives rise to Fermi shifts, which are determined by spin density delocalization. As both these mechanisms lead to similar changes in the spectra, the differentiation between them is usually not straightforward. In the case of the complexes studied, the separation is relatively easy to make owing to the remoteness of the apical substituent from the paramagnetic ion (five and more single bonds) that reduces direct spin delocalization on these groups, leading to the spectra dominated by pseudocontact shifts. At the same time, for nuclei in the chelate fragments, both the contact and pseudocontact interactions are possible.

Surprisingly, given the structural similarities of the complexes studied, the paramagnetic shifts in their NMR spectra (see Supporting Information, Figures S2−S9) were governed by very different mechanisms. The cobalt(II) complex demon-

dx.doi.org/10.1021/ic4029047 | Inorg. Chem. 2014, 53, 3062−3071

Table 1. Main Geometrical Parameters of the Pseudomacrobicyclic Metal Tris-Pyrazoloximates

	$[Zn(PzOx)_3(BC_6H_5)]Cl$	$[Co(PzOx)_3(BC_6H_5)]Cl$	$[Fe(PzOx)_3(BC_6H_5)]Cl$	$[Mn(PzOx)_3(BC_6H_5)]Cl$
metal ion	Zn^{2+}	Co^{2+} (hs)	Fe^{2+} (hs)	Mn^{2+} (hs)
Shannon radius (Å)	0.88	0.885	0.92	0.97
M−N1 (Å)	2.199(3)	2.132(3)	2.157(3)	2.273(3)
M−N2 (Å)	2.118(4)	2.129(4)	2.175(3)	2.221(3)
M−N4 (Å)	2.160(4)	2.134(4)	2.181(3)	2.237(3)
M−N5 (Å)	2.157(3)	2.159(3)	2.164(3)	2.228(3)
M−N7 (Å)	2.187(4)	2.125(4)	2.187(3)	2.280(3)
M−N8 (Å)	2.171(3)	2.127(3)	2.161(3)	2.211(3)
av M−N (Å)	2.17	2.13	2.18	2.24
B−O (Å)	1.490(6)−1.497(6) av 1.50	1.489(6)−1.503(7) av 1.49	1.484(5)−1.501(5) av 1.49	1.490(6)−1.510(6) av 1.50
N−O (Å)	1.374(4)−1.381(4) av 1.38	1.374(4)−1.392 (4) av 1.39	1.387(4)−1.388(4) av 1.39	1.366(4)−1.387(4) av 1.38
C═N (Å)	1.279(5)−1.288(6) av 1.28	1.285(7)−1.289(7) av 1.29	1.284(4)−1.342(4) av 1.32	1.280(6)−1.286(6) av 1.28
C−C (Å)	1.465(6)−1.476(6) av 1.47	1.458(6)−1.467(6) av 1.46	1.454(5)−1.466(5) av 1.46	1.464(4)−1.474(4) av 1.46
N═N (Å)	1.349(5)−1.352(5) av 1.35	1.343(6)−1.352(6) av 1.34	1.339(3)−1.352(3) av 1.35	1.347(4)−1.352(4) av 1.35
Cl···N (Å)	3.108(4)−3.156(4) av 3.13	3.103(4)−3.155(4) av 3.13	3.069(3)−3.126(3) av 3.10	3.068(4)−3.141(4) av 3.11
φ (deg)	1.3	1.5	3.8	1.9
α (deg)	36.7	37.1	36.4	35.8
h (Å)	2.58	2.57	2.56	2.60

strated very large values of the paramagnetic shifts of both the chelate and the capping fragments' nuclei, suggesting the significant contribution of the pseudocontact mechanism.[18] In the case of the iron(II) complex, large paramagnetic shifts were observed for the signals of the chelate fragments' nuclei, whereas those of the phenyl substituents are affected by the paramagnetic metallocenter only slightly. This corresponds to the prevalence of the contact contribution into the value of the paramagnetic shift with a very small pseudocontact input. For the manganese(II) complex with the electronic configuration d^5, no pseudocontact interaction is expected, so the observed shifts are entirely due to the direct delocalization of an unpaired electron over the polyazomethine pseudomacrobicyclic ligand, with paramagnetic broadening not allowing us to observe the signals of the carbon nuclei close to its encapsulated metal ion.

Thus, the magnetic properties of three paramagnetic complexes obtained strongly depend on the nature of the caged metal ion; the perspectives of the usage of these complexes as paramagnetic tags and single molecular magnets are currently under study in our groups.

IR spectra of the metal pseudomacrobicycles contain C═N, N−O, and B−O bond stretching vibrations characteristic of boron-capped α-dioximate macrobicyclic frameworks, together with the bands characteristic of the initial ligand PzOxH and metal scorpionates (first of all, ν(C═N) + ν(C═C) at approximately 1530 and 1670 cm^{-1}).

MALDI-TOF mass spectra of the pseudoclathrochelates of 3d metal ions with preferable octahedral N_6 coordination {i.e., iron, cobalt, and manganese(II) cations} contain intensive peaks of cationic pseudomacrobicyclic species $[M-Cl^-]^+$ as well as their pseudomacrocyclic derivatives with detachment of one pyrazoloximate fragment. The peak of cationic species, which resulted from a detachment of this fragment from a parent ionic associate, dominates in the spectrum of zinc(II) complex with a preferable tetrahedral N_4-coordination of its caged metal ion.

X-ray Diffraction Studies. Metal pseudoclathrochelates and their MN_6 coordination polyhedra as revealed by X-ray diffraction are shown in Figure 1; their main geometrical parameters and those of the hybrid iron(II) dioximatopyrazolates $FeBd_2(PzOx)(BF_2)(BF)$ and $FeBd_2(PzOx)(BF)_2$ (Scheme 1, **3** and **4**) are listed in Table 1 and Table S2 (see Supporting Information), respectively. The B−O, O−N, N═C, and C−C distances are characteristic of both the boron-capped tris-dioximate clathrochelate analogs[1] and such hybrid clathrochelatoscorpionates.[3] At the same time, the absence of one rigid apical group and the lability of the chloride−containing pseudocapping fragment allows for an expansion of the tripodal tris-pyrazolyl fragment of the pseudomacrobicyclic ligand in comparison with its boron-capped analog. The MN_6-coordination polyhedra possess a distorted trigonal prismatic geometry, with the distortion angles φ between their nonequivalent N_3-bases of approximately 0°. The average N···N distances in the boron-capped apical groups vary from 2.77 to 2.84 Å, which is substantially lower than those in the tripodal tris-pyrazolyl fragments (3.13−3.40 Å). Nevertheless, M−N distances fall in a narrow range for all these pseudoclathrochelates, and the encapsulated metal ions are situated in their geometrical centers. In the case of the cobalt(II) complex, this suggests the absence of a Jahn−Teller distortion, indicating a high-spin state (s = 3/2) of the caged cobalt(II) ion with the electronic configuration d^7.

The average M−N distances for the iron and manganese(II) pseudoclathrochelates are also characteristic of the high-spin complexes. These distances increase in a series of 3d transition metal ions from cobalt(II) (av 2.13 Å) to iron(II) (av 2.18 Å) and then to manganese(II) (av 2.24 Å), in agreement with Shannon radii for such high-spin hexacoordinate cations (Table 1) and experimental magnetometry data (vide supra). As a result, the average Fe−N distances (approximately 1.92 Å) for the low-spin hybrid iron(II) dioximatopyrazoloximates $FeBd_2(HPzOx)(BF_2)(BF)$ and $FeBd_2(PzOx)(BF)_2$[3] are substantially smaller than those of their high-spin analog $[Fe(PzOx)_3(BC_6H_5)]Cl$. Therefore, the pseudoclathrochelate species are able to undergo an expansion−contraction along their B···Fe···Cl rotation C_3 pseudoaxes, which makes it possible to encapsulate a relatively wide range of metal ions in their highest spin states. At the same time, unlike most of the polyazomethine iron and cobalt(II) clathrochelates[1] and their dioximatopyrazoloximate hybrid analogs (i.e., semi- and clathrochelatoscorpionates[3]) with the distortion angles φ in the range of 10−30°, the pseudoclathrochelates obtained do

dx.doi.org/10.1021/ic4029047 | Inorg. Chem. 2014, 53, 3062−3071

not undergo a rotational distortion around this axis: the corresponding φ values do not exceed 4° (Table 1).

Such expansion of the tripodal tris-pyrazoloximate framework allows for its capping (cross-linking) with chloride ion via three N−H···Cl hydrogen bonds that stabilize their pseudomacrobicyclic structures. The geometry of the resulting ionic associates is the same for all the X-rayed complexes, which may be divided into the following isostructural solvate pairs: $[Fe(PzOx)_3(BC_6H_5)]Cl\cdot C_2H_5OH$ and $[Mn(PzOx)_3(BC_6H_5)]Cl\cdot C_2H_5OH$, $[Co(PzOx)_3(BC_6H_5)]Cl\cdot CHCl_3$, and $[Zn(PzOx)_3(BC_6H_5)]Cl\cdot CHCl_3$.

The fourth lone electron pair of the chloride counterion allows it to be involved in intermolecular hydrogen bonding; the C−H···Cl-bonded dimers are observed in the crystals of all four pseudomacrobicyclic complexes (Figure 2). Only in the

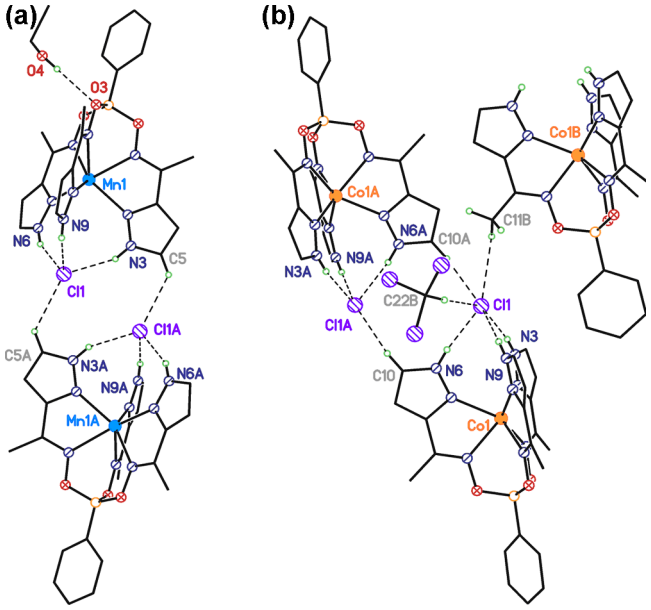

Figure 2. C−H···Cl-bonded dimers and other associates involving the chloride anion in the crystals (a) $[Mn(PzOx)_3(BC_6H_5)]Cl\cdot C_2H_5OH$ and (b) $[Co(PzOx)_3(BC_6H_5)]Cl\cdot CHCl_3$; the corresponding hydrogen bonds are depicted with dashed line. Hydrogen atoms that do not form such bonds are omitted for clarity.

case of the ethanol solvates $[Fe(PzOx)_3(BC_6H_5)]Cl\cdot C_2H_5OH$ and $[Mn(PzOx)_3(BC_6H_5)]Cl\cdot C_2H_5OH$, this chloride ion forms an almost tetrahedral H_4-environment with r_i(C···Cl) from 3.45 to 3.51 Å. In the crystals $[Co(PzOx)_3(BC_6H_5)]Cl\cdot CHCl_3$ and $[Zn(PzOx)_3(BC_6H_5)]Cl\cdot CHCl_3$, it also forms intermolecular C−H···Cl hydrogen bonds with the solvate chloroform molecule and with the methyl substituent at donor oxime fragment; such hydrogen bonds are up to 3.74 Å long.

Quantum Chemical Calculations and UV−vis−NIR Spectra. To explain why the pseudoclathrochelate $[Fe(PzOx)_3(BC_6H_5)]Cl$ has a high-spin ground state and to correlate its electronic structure with the experimental ^{57}Fe Mössbauer and UV−vis−NIR spectral data, we performed DFT and TDDFT calculations for all the possible spin states of this complex. It was found that the high-spin quintet state for the pseudoclathrochelate $[Fe(PzOx)_3(BC_6H_5)]Cl$ is indeed the lowest energy state for a DFT-optimized geometry, while its triplet and singlet states are much higher in energy (Table 2). As DFT-predicted orbital energies and compositions for the experimental (X-ray) and optimized geometries of a high-spin complex (s = 2) are very close (see Supporting Information, Table S3), only a brief description of the electronic structure of the optimized system is provided below, while the detailed discussion on the subject can be found in the Supporting Information. The DFT-optimized geometry converged into C_s point group, in agreement with the X-ray data for this pseudoclathrochelate. The MO diagram for the optimized complex $[Fe(PzOx)_3(BC_6H_5)]Cl$ is given in Figure 3, and MO

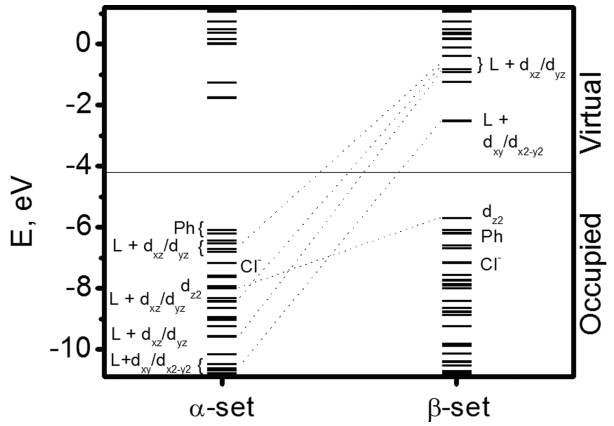

Figure 3. DFT-predicted molecular energy diagram for the high-spin state of the pseudoclathrochelate $[Fe(PzOx)_3(BC_6H_5)]Cl$.

compositions are summarized in Table 3 and Table S4 (see Supporting Information); the selected MOs are also shown in Figure 4, and the full set of these MOs can be found in Figures S10 and S11 (see Supporting Information).

The DFT-predicted electronic configuration of the high-spin pseudoclathrochelate complex $[Fe(PzOx)_3(BC_6H_5)]Cl$ is $(d_{z^2})^2$, $(d_{xy})^1$, $(d_{xz})^1$, $(d_{yz})^1$, $(d_{x^2-y^2})^1$, which can be expected for the pseudotrigonal ligand field created by the tripodal

Table 2. Experimental and DFT (B3LYP)-Predicted ^{57}Fe Mössbauer Spectral Parameters (mm s^{-1}) as well as the Relative Energies (E_{rel}, kcal mol^{-1}) and Spin Densities (au) for the Different Spin States of the Complex $[Fe(PzOx)_3(BC_6H_5)]Cl$

geometry	spin state	ρ_{spin} (Fe)	E_{rel}	ρ (Fe)	IS	V_{xx}	V_{yy}	V_{zz}	QS
					experimental				
					1.232 (298K)				3.447 (298K)
	s = 2				1.351 (77K)				4.141 (77K)
					DFT-predicted				
X-ray	s = 2	3.716		11 565.7551	1.355	−0.1794	−2.0926	2.2719	−4.093
DFT	s = 2	3.732	0.0	11 566.3942	1.065	−0.2618	−2.0753	2.3371	−4.149
DFT	s = 1	1.972	15.81	11 566.4738	1.040	0.2759	0.3323	−0.6082	0.987
DFT	s = 0	0.0	26.17	11 567.4078	0.753	0.4306	0.6765	−1.1071	1.808

dx.doi.org/10.1021/ic4029047 | Inorg. Chem. 2014, 53, 3062−3071

Table 3. DFT (B3LYP)-Predicted Compositions of Frontier MOs and Frontier MOs Region with Significant Iron Character for the Pseudoclathrochelate $[Fe(PzOx)_3(BC_6H_5)]Cl$, Based on Its Optimized Geometry

MO	E (eV)	Fe	Pyz 1[a]	Pyz 2[a]	Pyz 3[a]	Cl^-	BPh
			α-set composition, %				
112	−10.855	27.58	3.42	3.42	62.32	0.05	3.21
113	−10.806	23.64	32.97	32.97	6.67	0.04	3.71
114	−10.784	19.58	25.14	25.14	1.57	0.00	28.57
115	−10.771	18.13	13.81	13.81	0.65	0.01	53.59
116	−10.671	24.09	22.00	22.00	30.60	0.06	1.25
117	−10.614	19.76	33.94	33.94	7.56	0.10	4.71
120	−9.580	52.19	11.53	11.53	21.80	0.00	2.96
121	−9.561	52.25	18.66	18.66	5.83	0.00	4.61
128	−8.401	26.60	24.76	24.76	22.65	0.04	1.20
129	−8.306	22.58	25.62	25.62	19.36	0.02	6.79
130	−7.977	30.74	6.76	6.76	6.19	0.08	49.47
131	−7.927	49.21	7.10	7.10	3.59	0.42	32.58
133	−7.594	18.49	36.55	36.55	6.52	1.80	0.09
141	−6.429	18.65	33.23	33.23	8.68	0.04	6.16
144[b]	**−6.082**	**1.31**	**6.94**	**6.94**	**6.11**	**0.01**	**78.68**
145	**−1.760**	**4.07**	**45.36**	**45.36**	**2.79**	**0.14**	**2.29**
153	0.736	28.09	20.32	20.32	15.73	10.40	5.14
			β-set composition, %				
140[b]	**−5.683**	**87.78**	**4.31**	**4.31**	**2.69**	**0.45**	**0.45**
141	**−2.508**	**36.00**	**29.58**	**29.58**	**3.77**	**0.06**	**1.00**
142	−2.494	34.80	12.18	12.18	40.39	0.05	0.40
144	−0.914	31.93	27.51	27.51	10.23	0.22	2.59
145	−0.830	33.06	14.70	14.70	35.83	0.23	1.50
146	−0.387	40.73	17.85	17.85	23.26	0.01	0.31
150	0.329	22.19	20.14	20.14	31.16	0.07	6.30

[a]Pyz 1, Pyz 2, and Pyz 3 refer to three pyrazoloximate chelate fragments of the tripodal pseudomacrobicyclic ligand. [b]HOMO−LUMO are in bold font style.

pseudoencapsulating tris-pyrazoloximate ligand. In the α-set of DFT MOs, the 3d metal manifold contributed to several MOs (Table 3). The HOMO and HOMO-1 in the α-set are predominantly axial phenyl-centered MOs, while HOMO-2−HOMO-6 are predominantly pyrazolyl-centered π-orbitals. The LUMO to LUMO+5 are dominated by the pyrazolyl-centered π^*-orbitals. In the β-set, the HOMO has a predominantly d_{z^2} character (88%); HOMO-1 and HOMO-3 are dominated by the phenyl-centered π-orbitals, while HOMO-2 and HOMO-4−HOMO-5 are pyrazolyl-centered. The unoccupied iron 3d orbitals contribute significantly to LUMO and up to LUMO +13 (β-set).

The DFT-predicted ^{57}Fe Mössbauer spectral parameters of the high-spin complex $[Fe(PzOx)_3(BC_6H_5)]Cl$ are in excellent agreement with the experimental data (Table 2). More importantly, DFT-calculated IS and QS values for s = 1 and s = 0 states are very different from the experimental ones. The TDDFT approach was used to assign the experimental UV−vis−NIR spectrum of the complex $[Fe(PzOx)_3(BC_6H_5)]Cl$. Its TDDFT-predicted UV−vis−NIR spectrum is in a good agreement with the experimental one (Figure 5). Three types of transitions dominate in this spectrum: (i) intraligand $\pi-\pi^*$ transitions in its tripodal tris-pyrazoloximate pseudomacrobicyclic framework; (ii) phenyl-centered $\pi-\pi^*$ transitions; and (iii) $\pi-\pi^*$ transitions between the apical phenyl substituent and the pyrazoloximate chelate fragments (see Supporting Information, Table S5). Broad weak ($\varepsilon \approx 5$ mol^{-1} L cm^{-1}) band observed in the NIR region was tentatively assigned to the iron-localized ligand−field transition(s). Similar weak and Jahn−Teller broadened NIR transitions are characteristic of the high-spin iron(II) ion in its octahedral environment as well as in the tetragonally distorted systems with electronic configuration d^6.[19]

At the same time, the data for the trigonally distorted complexes of hexacoordinate high-spin iron(II) ion are surprisingly rare.[20] In a simplistic approach, the state diagram for quintet states of such d^6 systems is shown in Figure 6.[21] Given the expected small splitting between $^5A_1$ and ^5E (T_{2g}) states, one can assume the experimentally observed band at 905 nm to originate from the $^5A''$ ($^5E/^5E_g$) ← $^5A'$ ($^5A_1/^5T_{2g}$) and $^5A'$ ($^5E/^5E_g$) ← $^5A'$ ($^5A_1/^5T_{2g}$) transitions (bands 3 and 4), while the two lowest energy transitions $^5A''$ ($^5E/^5T_{2g}$) ← $^5A'$ ($^5A_1/^5T_{2g}$) and $^5A'$ ($^5E/^5T_{2g}$) ← $^5A'$ ($^5A_1/^5T_{2g}$) should be observed at very low energies (bands 1 and 2, Figure 6). In agreement with this model, the TDDFT approach predicts that the first two ligand−field transitions $d_{z^2} \rightarrow d_{xy}/d_{x^2-y^2}$ should be observed in the IR region (see Supporting Information, Table S5), while the NIR absorption band should consist of two contributions with $d_{z^2} \rightarrow d_{xz}/d_{yz}$ character. Although symmetry-allowed, these transitions were predicted to have zero oscillator strength, which is in excellent agreement with the experimental data. The TDDFT calculations also predict that the broad band at approximately 400 nm ($\varepsilon \approx 350$ mol^{-1} L cm^{-1}) has three major contributions (excited states 5−7, see Supporting Information, Table S5), which have significant phenyl(π) → Fe(d_{xz}/d_{yz}) and pyrazolyl(π)→ Fe(d_{xz}/d_{yz}) CT characters. Finally, numerous intensive bands in the range of 250−300 nm (see Supporting Information, Table S6) can be attributed to the allowed intraligand $\pi-\pi^*$ transitions in and between pyrazolyl and oxime fragments and phenyl substituent. We also observed

dx.doi.org/10.1021/ic4029047 | Inorg. Chem. 2014, 53, 3062−3071

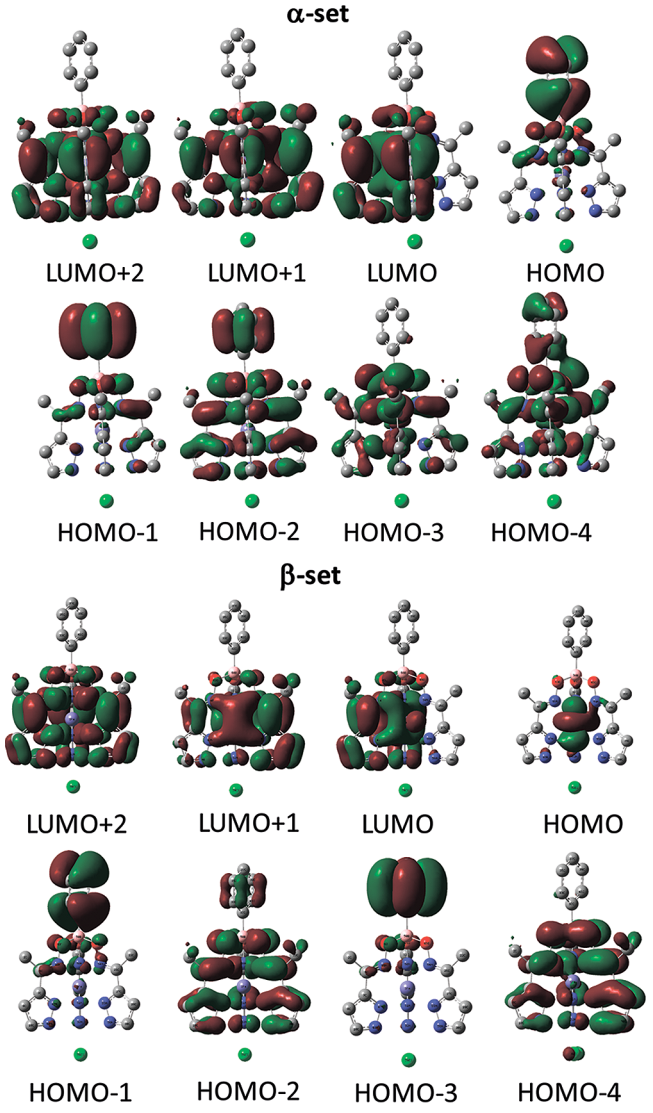

Figure 4. Selected surfaces for the frontier orbitals of the high-spin state (s = 2) of the pseudoclathrochelate $[Fe(PzOx)_3(BC_6H_5)]Cl$.

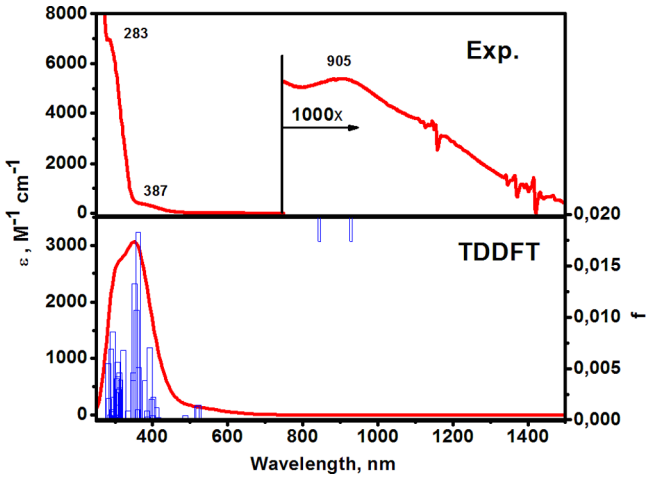

Figure 5. (top) Experimental and (bottom) TDDFT-calculated UV–vis–NIR spectra of $[Fe(PzOx)_3(BC_6H_5)]Cl$; two top vertical bars are the excited states 3 and 4 (f = 0).

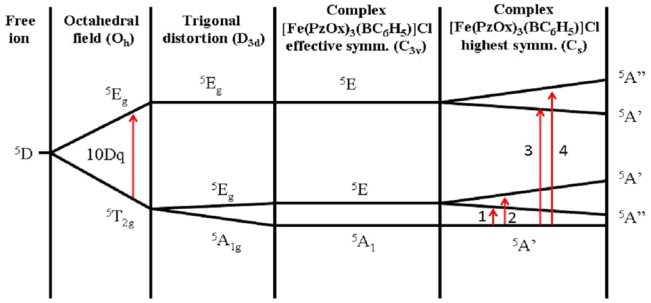

Figure 6. State diagram for quintet states of the high-spin pseudoclathrochelate $[Fe(PzOx)_3(BC_6H_5)]Cl$.

a similar low-intensive ligand–field band at 1071 nm in the vis–NIR spectrum of its cobalt-containing analog, being characteristic of d–d transitions in this ion.[19]

Electrochemistry. The electrochemical properties of the pseudomacrobicyclic complexes obtained were studied by cyclic voltammetry (CV). The peaks observed are characteristic of diffusion-controlled current processes (as it follows from the linear plot of I_p versus $v^{1/2}$, where v is scan rate). All these complexes undergo both the oxidation and the reduction in the potential range from −2000 to 2000 mV; the corresponding E values are summarized in Table S7 (see Supporting Information). The CV for the dichloromethane solution of the complex $[Fe(PzOx)_3(BC_6H_5)]Cl$ (Supporting Information, Figure S12) contains, in its anodic range, one-electron quasi-reversible wave with a ratio of the peak currents of direct and backward processes equal to 1 assigned to a metal-centered $Fe^{2+/3+}$ redox couple. This suggests the formation of oxidized iron(III)-containing pseudoclathrochelate species that are stable on the CV time scale. The cathodic range of this CV contains an irreversible $Fe^{2+/+}$ reduction wave; this irreversibility persists even at high potential scan rates (up to 1000 mV s^{-1}) and suggests fast chemical reactions of the reduced iron(I)-containing pseudoclathrochelate species. A similar redox behavior has been earlier described for an iron(II) macrocyclic complex $FeBd_2(HPzOx)(BF_2)(BF)$ and a clathrochelatoscorpionate $FeBd_2(PzOx)(BF)_2$ (Scheme 1, **3** and **4**).[3] CVs of these complexes also contain the anodic waves of metal-centered $Fe^{2+/3+}$ redox processes. The macrocyclic dioximato-pyrazoloximate $FeBd_2(HPzOx)(BF_2)(BF)$, lacking a rigid three-dimensional macrobicyclic framework that stabilizes the oxidized metallocenter, undergoes an irreversible oxidation, whereas its clathrochelate analog with a polyazomethine framework undergoes a quasi-reversible oxidation, suggesting the formation of its oxidized iron(III)-containing macrobicyclic form that is stable on the CV time scale.[3]

The oxidation of the pseudoclathrochelate $[Fe(PzOx)_3(BC_6H_5)]Cl$ is also quasi-reversible on this time scale, indicating that its pseudocross-linking chloride ion retains $Cl^-\cdots HN$ hydrogen bonds even in solution. This negatively charged apical cap stabilizes the oxidized form of this iron complex by forming a pseudomacrobicyclic hydrogen-bonded framework (vide supra), supplemented by strong electrostatic Coulombic interactions with triply positively charged oxidized metallocenter. Therefore, an opposite electrostatic effect of the negatively charged chloride counterion should be observed in the case of the metal-centered $Fe^{2+/+}$ reduction of the complex $[Fe(PzOx)_3(BC_6H_5)]Cl$. Indeed, as can be seen from Supporting Information, Figure S11, this process is irreversible. In general, the oxidation $Fe^{2+/3+}$ potentials of these iron(II)

dx.doi.org/10.1021/ic4029047 | Inorg. Chem. 2014, 53, 3062–3071

complexes (Supporting Information, Table S7) increase in a series: macrocyclic complex $FeBd_2(HPzOx)(BF_2)(BF)$ (950 mV) < pseudoclathrochelate $[Fe(PzOx)_3(BC_6H_5)]Cl$ (1300 mV) < clathrochelate $FeBd_2(PzOx)(BF)_2$ (1410 mV). The reverse is observed in the case of their reduction $Fe^{2+/+}$ potentials: macrocycle (−1420 mV) < pseudoclathrochelate (−1320 mV) < clathrochelate (−1075 mV). Thus, the formation of a macrobicyclic framework stabilizes their oxidized iron(III)-containing forms and destabilizes reduced iron(I)-containing complexes, but the reversibility of the corresponding redox process on the CV time scale increases in both these cases.

CV for a dichloromethane solution of the complex $[Co(PzOx)_3(BC_6H_5)]Cl$ (see Supporting Information, Figure S12) contains, in the cathodic range, a quasi-reversible wave assigned to the metal-centered $Co^{2+/+}$ reduction; this quasi-reversibility is caused by a structural rearrangement of the reduced pseudomacrobicyclic species on the CV time scale. The only irreversible wave in the anodic range at approximately 1800 mV can be assigned either to the metal-centered oxidation $Co^{2+/3+}$ or to the oxidation of the hydrogen-bonded chloride counterion. To assign this wave correctly, we studied the influence of the addition of *n*-tetrabutylammonium chloride to the dichloromethane solution of the complex $[Co(PzOx)_3(BC_6H_5)]Cl$ on the oxidation peak current: its value increased linearly with the concentration of this salt (Supporting Information, Figure S13). Note that the chloride anion in the dichloromethane solution of $((n\text{-}C_4H_9)_4N)Cl$ undergoes oxidation at the same potential value. Therefore, the irreversible wave at approximately 1800 mV in the CV of the pseudoclathrochelate $[Co(PzOx)_3(BC_6H_5)]Cl$ was assigned to the oxidation of its pseudocapping chloride ion, whereas the encapsulated cobalt(II) ion undergoes no oxidation in the potential range studied. Such unprecedented high stability of this oxidation state of the encapsulated cobalt ion has not been observed before for boron-capped tris-dioximate cobalt clathrochelates: all of them underwent oxidation at substantially lower potential values.[22] The dramatic difference in the redox behavior of the pseudoclathrochelate $[Co(PzOx)_3(BC_6H_5)]Cl$ and its tris-dioximate clathrochelate analogs may be explained by the low stability of the oxidized cobalt(III)-containing pseudomacrobicyclic tris-pyrazoloximate.

An irreversible reduction of the manganese(II) pseudoclathrochelate $[Mn(PzOx)_3(BC_6H_5)]Cl$ in its dichloromethane solution proceeds only at extremely high potential value (more than 2000 mV) and is followed by the destruction of its pseudomacrobicyclic framework. The CV of this complex (see Supporting Information, Figure S14) contains, in the anodic range, two irreversible oxidation waves at 950 and 1400 mV; the first was assigned to the metal-centered $Mn^{2+/3+}$ oxidation, being irreversible even at high scan rates (more than 1000 mV s^{-1}), while the second one was assigned to the oxidation of the products of irreversible chemical reactions following the complete destruction of the pseudoclathrochelate framework after its first oxidation to the unstable manganese(III)-containing pseudomacrobicyclic dicationic species.

In the case of the pseudoclathrochelate $[Zn(PzOx)_3(BC_6H_5)]Cl$ formed by a redox-inactive zinc(II) ion, the electrochemical oxidation and reduction are localized on the pseudoencapsulating polyazomethine ligand. As a result, the CV of this complex contains only irreversible multielectron waves assigned to ligand-localized redox processes.

We also performed the CV study of anion-exchange reactions of the complexes obtained in the presence of a substantial excess of bromide ions. Even in the case of a 50 M excess of *n*-tetrabutylammonium bromide, both the shape of the CV curve and the corresponding redox potential were the same. This suggests the absence of the anion-exchange reactions under these experimental conditions.

4. CONCLUSIONS

We found the first example of pseudoclathrochelate metal tris-pyrazoloximates obtained by efficient one-pot procedure in the presence of chloride anion. As it follows from X-ray diffraction data, this ion completes the formation of their pseudocapping apical fragment via strong hydrogen bonding with HN groups of three pyrazoloximate chelate moieties. While previously described boron-capped tris-dioximate clathrochelates and their hybrid clathrochelatoscorpionate analogs with covalently bonded rigid polyazomethine macrobicyclic ligands preferably encapsulate iron, ruthenium(II), and cobalt(II,III) ions in their low-spin states, a lability and the geometrical parameters of these new pseudoclathrochelate tris-pyrazolyl ligand systems allow for an efficient caging of various 3d metal ions in the high-spin states. This experimental result is found to be in excellent agreement with quantum-chemical DFT and TDDTF computations. According to CV data, such hydrogen-bonded cage complexes undergo irreversible or quasi-reversible electrochemical oxidations and reductions, and their capping chloride anion is inert to exchange reactions even in the presence of a high excess of bromide ion; thus, these pseudoclathrochelates have a high affinity toward chloride anions even in solution.

■ ASSOCIATED CONTENT

Ⓢ Supporting Information

CVs for the complexes studied, details of DFT calculations and the corresponding tables as well as UV−vis−NIR, electrochemical and crystallographic data, and full list of authors for reference 7. This material is available free of charge via the Internet at http://pubs.acs.org.

■ AUTHOR INFORMATION

Corresponding Author

*E-mail: voloshin@ineos.ac.ru.

Notes

The authors declare no competing financial interest.

■ ACKNOWLEDGMENTS

Financial support from the RFBR (Grants 12-03-90431, 13-03-00570, 13-03-00732, and 13-03-12155), RAS (Program 6), Council of the President of the Russian Federation (Grants MK-4842.2013.3 and SP-1292.2013.1), Russian State Atomic Energy Corporation "ROSATOM" (Project D.4f.43.90.13.1053) and the Marie Curie IRSES Scheme of the seventh EU Framework Program (Grant 295160) is greatly appreciated. V.N.N. would like to acknowledge support from Minnesota Supercomputing Institute and University of Minnesota Grant-in-Aid.

■ REFERENCES

(1) Voloshin, Y. Z.; Kostromina, N. A.; Kramer, R. *Clathrochelates: Synthesis, Structure and Properties*; Elsevier: Amsterdam, The Netherlands, 2002.

(2) (a) Belinski, J. A.; Squires, M. E.; Kuchna, J. M.; Bennet, B. A.; Grzybowski, J. J. *J. Coord. Chem.* **1988**, *19*, 159. (b) Grzybowski, J. J.; Alien, R. D.; Belinski, J. A.; Bieda, K. L.; Bish, T. A.; Finnegan, P. A.; Hartenstein, M. L.; Regitz, G. S.; Ryalls, D. M.; Squires, M. E.; Thomas, H. J. *Inorg. Chem.* **1993**, *32*, 5266. (c) Bieda, K. L.; Kranitz, A. L.; Grzybowski, J. J. *Inorg. Chem.* **1993**, *32*, 4209. (d) Voloshin, Y. Z.; Varzatskii, O. A.; Korobko, S. V.; Maletin, Y. A. *Inorg. Chem. Commun.* **1998**, *1*, 328. (e) Voloshin, Y. Z.; Stash, A. I.; Varzatskii, O. A.; Belsky, V. K.; Maletin, Y. A.; Strizhakova, N. G. *Inorg. Chim. Acta* **1999**, *284*, 180. (f) Voloshin, Y. Z.; Varzatskii, O. A.; Strizhakova, N. G.; Tkachenko, E. Y. *Inorg. Chim. Acta* **2000**, *299*, 104. (g) Voloshin, Y. Z.; Varzatskii, O. A.; Stash, A. I.; Belsky, V. K.; Bubnov, Y. N.; Vorontsov, I. I.; Potekhin, K. A.; Antipin, M. Y.; Polshin, E. V. *Polyhedron* **2001**, *20*, 2721. (h) Voloshin, Y. Z.; Varzatskii, O. A.; Korobko, S. V.; Antipin, M. Y.; Vorontsov, I. I.; Lyssenko, K. A.; Kochubey, D. I.; Nikitenko, S. G.; Strizhakova, N. G. *Inorg. Chim. Acta* **2004**, *357*, 3187. (i) Voloshin, Y. Z.; Varzatskii, O. A.; Tomilova, L. G.; Breusova, M. O.; Magdesieva, T. V.; Bubnov, Y. N.; Kramer, R. *Polyhedron* **2007**, *26*, 2733. (j) Voloshin, Y. Z.; Erdyakov, S. Y.; Makarenko, I. G.; Lebed, E. G.; Potapova, T. V.; Svidlov, S. V.; Starikova, Z. A.; Polshin, E. V.; Gurskii, M. E.; Bubnov, Y. N. *Russ. Chem. Bull.* **2007**, *56*, 1787. (k) Voloshin, Y. Z.; Makarov, I. S.; Vologzhanina, A. V; Polshin, E. V.; Monakov, Y. B.; Islamova, R. M.; Bubnov, Y. N. *Russ. Chem. Bull.* **2008**, *57*, 1215. (l) Voloshin, Y. Z.; Makarenko, I. G.; Erdyakov, S. Y.; Svidlov, S. V.; Vologzhanina, A. V.; Lebed, E. G.; Ignatenko, A. V.; Gurskii, M. E.; Bubnov, Y. N. *Inorg. Chim. Acta* **2010**, *363*, 395. (m) Belaya, I. G.; Svidlov, S. V.; Dolganov, A. V.; Zelinskii, G. E.; Potapova, T. V.; Vologzhanina, A. V.; Varzatskii, O. A.; Bubnov, Y. N.; Voloshin, Y. Z. *Dalton Trans.* **2013**, *42*, 13667. (n) Sabin, J. R.; Varzatskii, O. A.; Voloshin, Y. Z.; Starikova, Z. A.; Novikov, V. V.; Nemykin, V. N. *Inorg. Chem.* **2012**, *51*, 8362.

(3) Varzatskii, O. A.; Kats (Menkach), S. V.; Penkova, L. V.; Volkov, S. V.; Dolganov, A. V.; Vologzhanina, A. V.; Bubnov, Y. N.; Voloshin, Y. Z. *Eur. J. Inorg. Chem.* **2013**, 1987.

(4) Sheldrick, G. M. *SADABS,* v.2.01, Bruker/Siemens Area Detector Absorption Correction Program; Bruker AXS: Madison, Wisconsin, 1998.

(5) Spek, A. L. *Acta Crystallogr.* **2009**, *D65*, 148.

(6) Sheldrick, G. M. *Acta Crystallogr., Sect. A* **2008**, *64*, 112.

(7) Frisch, M. J; Trucks, G. W.; Schlegel, H. B.; Scuseria, G. E.; Robb, M. A.; Cheeseman, J. R.; Montgomery, Jr., J. A.; Vreven, T.; Kudin, K. N.; Burant, J. C.; Millam, J. M.; Iyengar, S. S.; Tomasi, J.; Barone, V.; Mennucci, B.; Cossi, M.; Scalmani, G.; Rega, N.; Petersson, G. A.; Nakatsuji, H.; Hada, M.; Ehara, M.; Toyota, K.; Fukuda, R.; Hasegawa, J.; Ishida, M.; Nakajima, T.; Honda, Y.; Kitao, O.; Nakai, H.; Klene, M.; Li, X.; Knox, J. E.; Hratchian, H. P.; Cross, J. B.; Adamo, C.; Jaramillo, J.; Gomperts, R.; Stratmann, R. E.; Yazyev, O.; Austin, A. J.; Cammi, R.; Pomelli, C.; Ochterski, J. W.; Ayala, P. Y.; Morokuma, K.; Voth, G. A.; Salvador, P.; Dannenberg, J. J.;. Zakrzewski, V. G.; Dapprich, S.; Daniels, A. D.; Strain, M. C.; Farkas, O.; Malick, D. K.; Rabuck, A. D.; Raghavachari, K.; Foresman, J. B.; Ortiz, J. V.; Cui, Q.; Baboul, A. G.; Clifford, S.;. Cioslowski, J.; Stefanov, B. B.; Liu, G.;. Liashenko, A.; Piskorz, P.; Komaromi, I.; Martin, R. L.; Fox, D. J.; Keith, T.; Al-Laham, M. A.; Peng, C. Y.; Nanayakkara, A.; Challacombe, M.; Gill, P. M. W.; Johnson, B.; Chen, W.; Wong, M. W.; Gonzalez, C.; Pople, J. A. *Gaussian 09*, Revision A.01; Gaussian, Inc.: Wallingford, CT, 2004.

(8) QMForge Program. http://qmforge.sourceforge.net/ (accessed 2013).

(9) (a) Becke, A. D. *J. Chem. Phys.* **1993**, *98*, 5648. (b) Lee, C.; Yang, W.; Parr, R. G. *Phys. Rev. B: Condens. Matter Mater. Phys.* **1988**, *37*, 785.

(10) McLean, A. D.; Chandler, G. S. *J. Chem. Phys.* **1980**, *72*, 5639.

(11) Wachters, A. J. H. *J. Chem. Phys.* **1970**, *52*, 1033.

(12) (a) Hehre, W. J.; Ditchfield, R.; Pople, J. A. *J. Chem. Phys.* **1972**, *56*, 2257. (b) Gordon, M. S. *Chem. Phys. Lett.* **1980**, *76*, 163.

(13) Nemykin, V. N.; Hadt, R. G. *Inorg. Chem.* **2006**, *45*, 8297.

(14) (a) Sessler, J. L.; Gale, P.; Cho, W.-S. *Anion Receptor Chemistry;* Stoddart, J. F., Ed.; Royal Society of Chemistry: Cambridge, UK, 2006. (b) Gimeno, N.; Vilar, R. *Coord. Chem. Rev.* **2006**, *250*, 3161. (b) Ballester, P. *Chem. Soc. Rev.* **2010**, *39*, 3810. (c) *Anion Coordination Chemistry;* Bowman-James, K.; Bianchi, A.; García-España, E., Eds.; Wiley-VCH: Weinheim, Germany, 2012.

(15) Carlin, R. L. *Magnetochemistry;* Springer: Berlin, Germany, 1986.

(16) Koehler, J.; Meiler, J. *Prog. Nucl. Magn. Reson. Spectrosc.* **2011**, *59*, 360.

(17) Bertini, I.; Luchinat, C.; Parigi, G. *Prog. Nucl. Magn. Reson. Spectrosc.* **2002**, *40*, 249.

(18) Voloshin, Y. Z.; Varzatskii, O. A.; Novikov, V. V.; Strizhakova, N. G.; Vorontsov, I. I.; Vologzhanina, A. V.; Lyssenko, K. A.; Romanenko, G. V.; Fedin, M. V.; Ovcharenko, V. I.; Bubnov, Y. N. *Eur. J. Inorg. Chem.* **2010**, 5401.

(19) Lever, A. B. P. *Inorganic Electronic Spectroscopy;* Elsevier: Amsterdam, The Netherlands, 1984.

(20) (a) Fleisch, J.; Guetlich, P.; Hasselbach, K. M.; Mueller, W. *Inorg. Chem.* **1976**, *15*, 958. (b) Chang, H. R.; McCusker, J. K.; Toftlund, H.; Wilson, S. R.; Trautwein, A. X.; Winkler, H.; Hendrickson, D. N. *J. Am. Chem. Soc.* **1990**, *112*, 6814.

(21) Methodology. In *Inorganic Electronic Structure and Spectroscopy;* Solomon, E. I.; Lever, A. B. P., Eds; Wiley: Weinhiem, Germany, 1999; Vol. *I*.

(22) (a) Voloshin, Y. Z.; Varzatskii, O. A.; Belov, A. S.; Starikova, Z. A.; Dolganov, A. V.; Novikov, V. V.; Bubnov, Y. N. *Inorg. Chim. Acta* **2011**, *70*, 322. (b) Voloshin, Y. Z.; Belaya (Makarenko), I. G.; Belov, A. S.; Platonov, V. E.; Maksimov, A. M.; Vologzhanina, A. V.; Starikova, Z. A.; Dolganov, A. V.; Novikov, V. V.; Bubnov, Y. N. *Dalton Trans.* **2012**, *41*, 737. (c) Voloshin, Y. Z.; Belov, A. S.; Vologzhanina, A. V.; Aleksandrov, G. G.; Dolganov, A. V.; Novikov, V. V.; Varzatskii, O. A.; Bubnov, Y. N. *Dalton Trans.* **2012**, *41*, 6078. (d) Dolganov, A. V.; Belov, A. S.; Novikov, V. V.; Vologzhanina, A. V.; Mokhir, A.; Bubnov, Y. N.; Voloshin, Y. Z. *Dalton Trans.* **2013**, *42*, 4373. (e) Belov, A. S.; Dolganov, A. V.; Novikov, V. V.; Vologzhanina, A. V.; Fedin, M. V.; Kuznetsov, E. V.; Bubnov, Y. N.; Voloshin, Y. Z. *Inorg. Chem. Commun.* **2013**, *29*, 160.